A Theory of Vertical Momentum Transport by Organized Cumulus Clouds

Anning Cheng and David A. Randall

Department of Atmospheric Science
Colorado State University
Fort Collins, CO 80523

Submitted to *the Journal of the Atmospheric Sciences*

April 24, 2001

Corresponding author's address:

Anning Cheng
Department of Atmospheric Science
Colorado State University
Fort Collins, CO 80523
Email: anning@atmos.colostate.edu

Abstract

A parameterization of cumulus momentum transport is proposed. An important feature of the parameterization is the inclusion of the perturbation pressure-gradient force induced by interactions between the updraft and the environmental wind. The orientation, aspect ratio, and phase speed of the organized convection are determined. These quantities depend on the vertical wind shear, the stratification and the heating and cooling rates due to various processes.

GATE, ARM, EMEX, SCSMEX, and TOGA COARE data are used to test the theory. Results show that: 1) the predicted orientation, aspect ratio, and phase speed of organized convection agree well with the observations. 2) the vertical momentum transport is sensitive to the orientation of the cumulus clouds; 3) the momentum transport due to the perturbation pressure-gradient force tends to be upgradient and to cancel with the vertical momentum advection and detrainment effects.

1. Introduction

An important effect of cumulus convection is the vertical redistribution of momentum. Stevens (1979) found large momentum-budget residuals in his analysis of an averaged easterly wave during GATE (the Global Atmospheric Research Program's Atlantic Tropical Experiment) Phase III. A distinct residual dipole pattern in the upper troposphere over deep convection was also found in a vorticity budget calculation using GATE phase III data (Tollerud and Esbensen, 1983; Sui and Yanai, 1986). Momentum transport by cumulus clouds has also been studied using numerical simulations (Moncrieff and Green, 1972; Soong and Tao, 1984; Tao and Soong,1986; Moncrieff, 1992; Zhang and Cho, 1991; Wu and Yanai, 1994).

The importance of organized cumulus clouds for momentum transport has been studied since the 1970s. Linear Mesoscale Convective Systems (MCSs), in which the clouds are organized along a line (i. e., a squall line), and nonlinear MCSs, in which the clouds are organized as a quasi-circular mass, produce totally different vertical momentum transports. Asai (1970) found that the air motion in longitudinal rolls is three-dimensional and results in a downgradient flux of horizontal momentum, and that the air motion in transverse rolls results in upgradient horizontal momentum transport. Lemone and Jorgensen (1991) reported that, for the cases they studied, the line-normal momentum transport is downgradient in the lower troposphere and upgradient in the upper troposphere. Wu and Yanai (1994) found from AVE-SESAME (Atmospheric Variability Experiment -- Severe Environmental Storms and Mesoscale Experiment) and OK PRE-STORM (Oklahoma-Kansas Preliminary Regional Experiment for STORM-Central) data and numerical simulations that the vertical momentum transport associated

with nonlinear MCSs, which they called mesoscale convective complexes[1] (MCCs), is downgradient in the upper layer. Vertical momentum transport of the component normal to a squall line is upgradient, and the transport of the component parallel to the line is downgradient in the upper layer. Stevens (1979), Tollerud and Esbensen (1983), Lemone et al. (1984), and Sui and Yanai (1986) found downgradient transport in nonlinear MCSs using various data sets.

Meanwhile Moncrieff and Green (1972), Tollerud and Esbensen (1983), Lafore et al. (1988), LeMone and Jorgensen (1991), and Gallus and Johnson (1992) found that horizontal momentum is not conserved inside convective updrafts. They suggested that upgradient momentum transport is associated with convective-scale pressure effects. The subsidence of the environmental air associated with the cumulus mass flux, the detrainment of momentum from clouds, and the convective-scale horizontal pressure-gradient force are the three physical factors that determine the effects of cumulus clouds on the momentum budget. The perturbation pressure-gradient force is mainly produced by the interactions of updraft and the vertical wind shear. This has been confirmed by many observations and numerical simulations (Rotunno and Klemp, 1982; Hane and Ray, 1985; Lin et al. 1986; Lemone et al. 1988; Weisman et al. 1988; Jorgensen et al. 1991; Wu and Yanai, 1994). According to theory and analyses of numerical simulations (Wu and Yanai 1994, Moncrieff 1992), the convective-scale horizontal pressure-gradient force is an important factor influencing the momentum transport.

[1.] Johnson and Hamilton (1988) pointed out that some MCCs have linear structure.

Many attempts have been made to parameterize the dynamical effects of cumulus convection in terms of large-scale variables. However, the convective-scale horizontal pressure-gradient force was ignored in most studies before 1990. Detrainment and environmental subsidence can partially explain the observed momentum budget residuals, but large systematic differences occur when the vertical shear is strong (Sui et al. 1989).

Moncrieff's (1992) "archetypal" two-dimensional model is based on a set of conservation principles and integral constraints. Three configurations are considered: the jump updraft, an overturning updraft in the rear of the system and an overturning updraft in the front. Some studies have shown that the momentum transport predicted by this idealized model is consistent with observations for low values of the Richardson number[1] and in the absence of extensive stratiform clouds (Moncrieff 1992 and Lemone and Moncrieff 1994). Application of the model requires a method to activate the scheme, the scale of the grid, the line orientation, the line speed, the line-parallel momentum transport, the depth of the cloud, the height of the jump updraft, and the height of the rear overturning current. Most of these parameters are not available in general circulation models (GCMs).

Zhang and Cho (1991a, 1991b) and Zhang and McFarlane (1995) developed a parameterization of convective momentum transport including the effects of the perturbation pressure field. They did not distinguish between the nonlinear MCS case and the linear MCS case,

[1.] Defined as the ratio of the Convective Available Potential Energy (CAPE) to the kinetic energy associated with the shear.

and the orientation of the organized convection was not considered. Their study accounts for the effects of down-gradient convective momentum transport.

Wu and Yanai (1994) developed a parameterization that includes the effects of the convective-scale pressure-gradient force acting on the updraft. Their approach has a clear physical interpretation and captures the main characteristics of the perturbation pressure-gradient force in terms of the vertical wind shear, the cloud mass flux, and the orientation of the organized convection. Both up-gradient and down-gradient vertical momentum transports can be explained with their scheme. However, the scheme can not determine the orientation of the organized convection.

The objectives of this paper are: 1) to propose a cumulus momentum transport parameterization that includes the effects of the convective-scale horizontal pressure-gradient force, 2) to develop a method to determine the orientation, aspect ratio, size and propagation speed of the organized convection, and 3) to determine the effects of cumulus momentum transport on the environmental wind field.

2. Perturbation pressure gradient force

2.1 The perturbation pressure-gradient force for organized clouds

The ideas presented here are an extension of the work of Wu and Yanai (1994), Yau (1979) and Holton (1973). Neglecting the Coriolis and the friction terms, a diagnostic pressure equation can be derived under the anelastic approximation:

$$-\nabla^2 p' = 2\rho\left(\frac{\partial \bar{u}}{\partial z}\frac{\partial w}{\partial x} + \frac{\partial \bar{v}}{\partial z}\frac{\partial w}{\partial y}\right) + \rho\left[\left(\frac{\partial u'}{\partial x}\right)^2 + \left(\frac{\partial v'}{\partial y}\right)^2 + \left(\frac{\partial w}{\partial z}\right)^2\right] + 2\rho\left[\frac{\partial u'}{\partial z}\frac{\partial w}{\partial x} + \frac{\partial v'}{\partial z}\frac{\partial w}{\partial y} + \frac{\partial u'}{\partial y}\frac{\partial v'}{\partial x}\right]$$

$$-\frac{\partial \rho B}{\partial z} + \frac{w^2}{\rho}\left(\frac{\partial \rho}{\partial z}\right)^2 - w^2\frac{\partial^2 \rho}{\partial z^2}. \qquad (1)$$

Here $\nabla^2 = \frac{\partial^2}{\partial x^2} + \frac{\partial^2}{\partial y^2} + \frac{\partial^2}{\partial z^2}$, $\bar{u}$ and $\bar{v}$ are the horizontal components of the environmental wind, w is the vertical velocity, and ρ is the air density. u' and v' are the cloud-scale perturbation velocity components, $u' = u - \bar{u}$, $v' = v - \bar{v}$, where u and v are the horizontal components of the mesoscale wind. $B \equiv g\frac{T_v - \overline{T_v}}{\overline{T_v}}$ is the buoyancy, where T_v is the virtual temperature for the clouds and $\overline{T_v}$ is the virtual temperature of the environment. The first two terms on the right-hand

side of (1) are due to the effects of the vertical wind shear. The following six terms are nonlinear. The ninth term is the vertical gradient of the buoyancy. The last two terms are due to the vertical change of the density. We can write

$$p' = p'_{shear} + p'_{nonlinear} + p'_{buoyancy} + p'_{density}. \quad (2)$$

In order to calculate the perturbation pressure-gradient force, we consider organized convective clouds as shown in ***Fig. 1***. The clouds are assumed to be organized in the shape of an ellipse which makes an angle θ with the x-axis. This is a mesoscale system with individual convective clouds embedded in it. The derivation below applies to a "smoothed" mesoscale envelope of the convection, so that individual convective cells are not represented. By adjusting the length of the major and minor axes of the ellipse, we can make the elliptical cloud system represent either a linear or a nonlinear MCS.

For this system, we assume that the shape of the vertical velocity distribution is

$$w = \hat{w}\sin kx'\sin ky'\sin mz \ , \ 0 \le \ kx', ly', mz \ \le \pi, \quad (3)$$

where $\hat{w}$ is the maximum mesoscale vertical velocity within the ellipse and k, l and m are the wave numbers characterizing the scales of the organized convective mesoscale system. At the upper and lower boundaries, $w = 0$. Equation (3) assumes a smooth, rounded profile for the vertical velocity inside the mesoscale region. We also assume that the mesoscale horizontal velocity distribution is described by:

$$u' = v_0(z)\cos(kx')\sin(ly')\cos(mz)\ ,\ 0 \le \quad kx', ly', mz \ \le \pi, \tag{4}$$

$$v' = v_0(z)\sin(kx')\cos(ly')\cos(mz)\ ,\ 0 \le \quad kx', ly', mz \ \le \pi. \tag{5}$$

In (4) and (5), $v_0(z)$ is the magnitude of the mesoscale horizontal velocity. At the boundary of the mesoscale system, u' and v' are assumed to be zero. Lower-level convergence and upper-level divergence can occur with this kind of horizontal velocity distribution. Substituting (3), (4) and (5) into the continuity equation

$$\frac{\partial u'}{\partial x} + \frac{\partial v'}{\partial y} + \frac{\partial w}{\partial z} + \frac{1}{\rho}\frac{\partial \rho}{\partial z}w = 0\ , \tag{6}$$

we find that:

$$v_0(z) = \frac{\hat{w}\left[m + \frac{1}{\rho}\frac{\partial \rho}{\partial z}\tan(mz)\right]}{k + l}. \tag{7}$$

We now substitute (3), (4), (5) and (7) into the terms on the right-hand side of (1) in order to derive expressions for the perturbation pressure-gradient force. First, substituting (3) into the first two terms of (1), we obtain an expression for p'_{shear}:

$$\frac{p'_{shear}}{\rho} = \frac{2}{(k^2 + l^2 + m^2)}\left[\frac{\partial \bar{u}}{\partial z}k\cos(kx')\sin(ly') + \frac{\partial \bar{v}}{\partial z}l\sin(kx')\cos(ly')\right]\hat{w}\sin(mz). \tag{8}$$

According to (8), this component of the perturbation pressure depends on the vertical wind shear, the vertical wind speed and the orientation of the system. An expression for the pressure-gradient force can be derived from :

$$-\sigma\left(\frac{1}{\rho}\cdot\frac{\partial p'}{\partial x'}\right)_{\sigma,\,shear} = \frac{\nu_k}{\rho}\cdot\left(\frac{\partial \bar{u}}{\partial z}\right)M\,, \tag{9}$$

$$-\sigma\left(\frac{1}{\rho}\cdot\frac{\partial p'}{\partial y'}\right)_{\sigma,\,shear} = \frac{\nu_l}{\rho}\cdot\left(\frac{\partial \bar{v}}{\partial z}\right)M\,, \tag{10}$$

$$-\sigma\left(\frac{1}{\rho}\cdot\frac{\partial p'}{\partial z}\right)_{\sigma,\,shear} = 0\,. \tag{11}$$

Here $\nu_k = \dfrac{2k^2}{k^2+l^2+m^2}$, $\nu_l = \dfrac{2l^2}{k^2+l^2+m^2}$, and $M = \rho\sigma\bar{w}_s$ is the mass flux for this system, where σ is the area of the system and $\bar{w}_s$ is the area-average vertical velocity. The notation $(\ )_\sigma$ denotes an area average over the ellipse. Equations (9) and (10) are the same as those derived by Wu and Yanai (1994), but their result is applied to individual cumulus clouds.

Now substitute (3), (4), (5) and (7) into the nonlinear terms on the right-hand side of (1). The result is

$$p'_{nonlinear} = \left\{\rho[v_0^2(k^2+l^2)+\hat{w}^2m^2](\sin kx'\sin ly'\cos mz\right)^2$$

$$-2\rho v_0 mk\hat{w}(\cos kx'\sin ly'\sin mz)^2 +$$

$$2\rho v_0[-ml\hat{w}(\sin kx'\cos ly'\sin mz)^2 + klv_0(\cos kx'\cos ly'\cos mz)^2]\Big\}/(k^2+l^2+m^2). \quad (12)$$

This gives an expression for the perturbation pressure-gradient force due to nonlinear effects:

$$-\sigma\left(\frac{1}{\rho}\cdot\frac{\partial p'}{\partial x'}\right)_{\sigma,\,nonlinear} = 0, \quad (13)$$

$$-\sigma\left(\frac{1}{\rho}\cdot\frac{\partial p'}{\partial y'}\right)_{\sigma,\,nonlinear} = 0, \quad (14)$$

$$-\sigma\left(\frac{1}{\rho}\cdot\frac{\partial p'}{\partial z}\right)_{\sigma,\,nonlinear} = \frac{\sigma}{4\rho(k^2+l^2+m^2)}\Bigg[(k+l)^2\frac{\partial\rho v_0^2 cos^2 mz}{\partial z} + \hat{w}^2 m^2\frac{\partial\rho cos^2 mz}{\partial z}$$

$$-2wm(k+l)\frac{\partial\rho v_0 sin^2 mz}{\partial z}\Bigg]. \quad (15)$$

We see from (13) and (14) that for this kind of velocity distribution, the perturbation horizontal pressure-gradient force due to the nonlinear effects is zero. The nonlinear effects do contribute to the vertical component of the perturbation pressure-gradient force.

For the buoyancy term, we assume that $B = B_0(z)\sin(kx')\sin(ly')$, and substitute into (1):

$$p'_{buoyancy} = \frac{\sin(kx')\sin(ly')}{(k^2 + l^2 + m^2)} \frac{\partial(\rho B_0)}{\partial z}. \tag{16}$$

An expression for the perturbation pressure-gradient force due to the buoyancy term can be derived as follows:

$$-\sigma\left(\frac{1}{\rho} \cdot \frac{\partial p'}{\partial x'}\right)_{\sigma,\, buoyancy} = 0, \tag{17}$$

$$-\sigma\left(\frac{1}{\rho} \cdot \frac{\partial p'}{\partial y'}\right)_{\sigma,\, buoyancy} = 0, \tag{18}$$

$$-\sigma\left(\frac{1}{\rho} \cdot \frac{\partial p'}{\partial z}\right)_{\sigma,\, buoyancy} = \frac{4\sigma}{\pi^2(k^2 + l^2 + m^2)} \frac{1}{\rho} \frac{\partial^2(\rho B_0)}{\partial z^2}. \tag{19}$$

This shows that the buoyancy force has no effects on the perturbation horizontal pressure-gradient force, but does affect the perturbation vertical pressure-gradient force.

Finally, substitute (3) into the last two terms (the density-variation terms) on the right-hand side of (1) to obtain:

$$p'_{density} = \frac{\hat{w}^2 sin^2 kx' sin^2 ly' sin^2 mz}{(k^2 + l^2 + m^2)} \left[\frac{1}{\rho}\left(\frac{\partial \rho}{\partial z}\right)^2 - \frac{\partial^2 \rho}{\partial z^2}\right]. \tag{20}$$

This leads to:

$$-\sigma\left(\frac{1}{\rho}\cdot\frac{\partial p'}{\partial x'}\right)_{\sigma,\,density} = 0\,, \tag{21}$$

$$-\sigma\left(\frac{1}{\rho}\cdot\frac{\partial p'}{\partial y'}\right)_{\sigma,\,density} = 0\,, \tag{22}$$

$$-\sigma\left(\frac{1}{\rho}\cdot\frac{\partial p'}{\partial z}\right)_{\sigma,\,density} = \frac{\sigma}{(k^2+l^2+m^2)}\frac{\hat{w}^2}{4\rho}\frac{\partial\left\{sin^2 mz\left[\frac{1}{\rho}\left(\frac{\partial\rho}{\partial z}\right)^2-\frac{\partial^2\rho}{\partial z^2}\right]\right\}}{\partial z}\,. \tag{23}$$

We see that the density variations do not affect the horizontal perturbation pressure-gradient force, but do affect the vertical perturbation pressure-gradient force.

All of the above formulae have been derived in (x', y') coordinates. We need an expression in (x, y) coordinates. The vertical perturbation pressure-gradient force need not be changed. The horizontal perturbation pressure-gradient force is transformed to:

$$-\sigma\left(\frac{1}{\rho}\cdot\frac{\partial p'}{\partial x}\right)_{\sigma} = \frac{\nu_k}{\rho}\cdot\left(\frac{\partial\bar{u}}{\partial z}\right)M\cos\theta - \frac{\nu_l}{\rho}\cdot\left(\frac{\partial\bar{v}}{\partial z}\right)M\sin\theta\,, \tag{24}$$

$$-\sigma\left(\frac{1}{\rho}\cdot\frac{\partial p'}{\partial y}\right)_{\sigma} = \frac{\nu_k}{\rho}\cdot\left(\frac{\partial\bar{u}}{\partial z}\right)M\sin\theta + \frac{\nu_l}{\rho}\cdot\left(\frac{\partial\bar{v}}{\partial z}\right)M\cos\theta\,. \tag{25}$$

Here θ is the unknown orientation angle.

In contrast to Yau's (1979) approach, our approach describes a mesoscale convective system inside a grid box, while Yau's described individual convective cells. Although we use horizontal and vertical velocity distributions similar to those used by Yau, we use the anelastic approximation in the continuity equation, which is more accurate than the Bousinesq approximation used by Yau.

2.2 The orientation of the organized convective cumulus clouds

The unknowns in formulae (15), (19), (23), (24) and (25) are the parameters describing the scale and orientation of the system, i.e. k, l, m, θ. Little observational and theoretical work has been done on this topic.

Various Richardson numbers (Moncrieff and Green, 1972; Ludlam, 1980; Weisman and Klemp, 1982; Seitter and Kuo, 1983) have been used to classify different types of thunderstorms. Supercell thunderstorms tend to occur for small Richardson numbers, multicell storms for moderate Richardson numbers and air-mass thunderstorms for large Richardson numbers. Using SESAME, PRE-STORM and GATE data, Wu and Yanai (1994) found that large low-level vertical shear is an important factor distinguishing nonlinear MCSs from linear MCSs, although the convective available potential energy also has some influence. The studies mentioned above discuss both dynamic and thermodynamic factors affecting the types of storms. These two classes of factors do influence the organization of convective clouds, but a method is needed to calculate the orientation of organized convection.

Asai (1970, 1972) reported that the preferred unstable perturbation is the convective roll which is aligned with the vertical shear of the modified basic flow. Weisman and Klemp (1984)'s work shows that a spectrum of storm types exists, with different types of directionally varying wind shears: short-lived single cells exist with low shear, multicell storms with intermediate shear and supercells with high shear. Barnes and Sieckman (1984) classified tropical mesoscale cloud lines occurring in GATE into two different types---fast-movers and slow-movers. For the slow-movers, the principal component of the low-level shear is parallel to the squall line; while for fast-movers the low-level wind shear lies perpendicular to the squall line. Bluestein and Jain (1985) and Bluestein et al. (1987) noted that Oklahoma convective lines tend to be parallel to the low-level shear. Alexander and Young (1992) using the Equatorial Mesoscale Experiment (EMEX) data, Lemone et al. (1998) using the Tropical Ocean Global Atmosphere Coulped Ocean-Atmosphere Response Experiment (TOGA COARE) data, and Johnson and Keenan (2001) using South China Sea Monsoon Experiment (SCSMEX) data found that both the low-level and middle-level shear affect the organization of MCSs. Shear-perpendicular lines tend to develop if the shear exceeds a certain critical value close (4 m s^{-1}) at low levels and shear-parallel lines tend to develop if the low-level shear is less than the critical value and the middle-level shear (800-400 hPa) exceeds 5 m s^{-1}. When the shear at both levels is large, the orientation of the primary convective band is determined by the low-level shear. The mechanism for the lines perpendicular to low-level shear is that the convection organizes itself in order to establish a balance between the low-level wind shear and the cold pool when the low-level shear is very large (Rotunno et al. 1988). The mechanism for the shear parallel lines is not well understood.

The studies cited above emphasize the importance of vertical wind shear, especially at low levels. Their most important findings are that lines can be parallel to or perpendicular to the vertical wind shear vector. However, they did not give a method to distinguish these two cases.

We now outline an approach to determine the orientation of the convection. Using the anelastic approximation, the prognostic equations governing the cumulus cloud system can be written as:

$$\frac{\partial u'}{\partial t} + \bar{u}\frac{\partial u'}{\partial x} + \bar{v}\frac{\partial u'}{\partial y} + w'\frac{\partial \bar{u}}{\partial z} + \frac{\partial}{\partial x}\left(\frac{p'}{\bar{\rho}}\right) = 0, \tag{26}$$

$$\frac{\partial v'}{\partial t} + \bar{u}\frac{\partial v'}{\partial x} + \bar{v}\frac{\partial v'}{\partial y} + w'\frac{\partial \bar{v}}{\partial z} + \frac{\partial}{\partial y}\left(\frac{p'}{\bar{\rho}}\right) = 0, \tag{27}$$

$$\frac{\partial w'}{\partial t} + \bar{u}\frac{\partial w'}{\partial x} + \bar{v}\frac{\partial w'}{\partial y} + \frac{\partial}{\partial z}\left(\frac{p'}{\bar{\rho}}\right) - \frac{\theta'}{\bar{\theta}}g = 0, \tag{28}$$

$$\frac{\partial u'}{\partial x} + \frac{\partial v'}{\partial y} + \frac{\partial w'}{\partial z} + \frac{1}{\bar{\rho}}\frac{\partial \bar{\rho}}{\partial z}w' = 0, \tag{29}$$

$$\frac{\partial}{\partial t}\left(\frac{\theta'}{\bar{\theta}}\right) + \bar{u}\frac{\partial}{\partial x}\left(\frac{\theta'}{\bar{\theta}}\right) + \bar{v}\frac{\partial}{\partial y}\left(\frac{\theta'}{\bar{\theta}}\right) + \frac{N^2}{g}w' = \dot{\Theta}'. \tag{30}$$

Here $\boldsymbol{v}'$ and θ' are the perturbation momentum and potential temperature, and $\bar{\boldsymbol{v}}$, $\bar{\theta}$ and $\bar{\rho}$ are the average velocity, potential temperature and the average density, respectively. N^2 is the Brunt-Vaisalla frequency. $\dot{\Theta}'$ is the perturbation heating and cooling of the cloud due to various processes, such as the cloud microphysical processes, entrainment, detrainment and radiation effects. We assume that $\dot{\Theta}' = \frac{N_0^2 w'}{g}$. Combining the two terms of (30) that involve w', we get one term $\frac{N_1^2 w'}{g}$, where the coefficient N_1^2 encompasses the thermodynamic properties of the clouds and the environment, to which the condensation effects contribute a lot. In this paper, we assume that

$$N_1^2 = \frac{g}{\bar{\theta}_e}\frac{\partial \overline{\theta_e}}{\partial z}, \tag{31}$$

where $\overline{\theta_e}$ is the equivalent potential temperature of the environment.

To simplify the above equations, we assume that

$$\bar{u} = u_0 + c_{01}(z - z_0) \text{ and } \bar{v} = v_0 + c_{02}(z - z_0), \tag{32}$$

where u_0 and v_0 are the components of horizontal velocity at a reference level, z_0 is the height of the reference level, $c_{01} = \frac{\partial \bar{u}}{\partial z}$ and $c_{02} = \frac{\partial \bar{v}}{\partial z}$ are constants. Such quasi-linear horizontal velocity profiles are common in the lower troposphere and are very important for the orientation of organized convective clouds. We also assume that $c_{03} = \frac{1}{\bar{\rho}}\frac{\partial \bar{\rho}}{\partial z}$ is a constant.

We use the WKBJ method to solve (26)-(30) with the above assumptions. The first step is non-dimensionalization. For convective systems, the following relationships exist:

$$(x, y) = L(x^*, y^*),\ (z) = H(z^*),\ (u', v', w', \bar{u}, \bar{v}, u_0, v_0) = U(u'^*, v'^*, w'^*, \bar{u}^*, \bar{v}^*, u_0^*, v_0^*),$$

$$(c_{01}, c_{02}) = \alpha(c_{01}^*, c_{02}^*),\ \frac{p'}{\bar{\rho}} = U^2\frac{p'^*}{\bar{\rho}^*},\ \frac{1}{\bar{\rho}}\frac{\partial \bar{\rho}}{\partial z} = \frac{1}{H}\frac{1}{\bar{\rho}^*}\frac{\partial \bar{\rho}^*}{\partial z^*},$$

$$\frac{\theta'}{\bar{\theta}} = \left(\frac{\theta'}{\theta_0}\right)\frac{\theta'^*}{\bar{\theta}^*},\ \mu_1^2 = \frac{LN_1^2}{g}\frac{\theta_0}{\theta'},\ t = \frac{L}{U}t^*,\ \mu_2^2 = \frac{gL}{U^2}\frac{\theta_0}{\theta'}. \qquad (33)$$

Here L and H are used to scale the horizontal and vertical dimensions of the organized mesoscale system respectively, which are assumed to be of the same order. U is the scale for the environmental and cloud velocities. Superscript "*" denotes a non-dimensional variable, $\alpha = \frac{U}{H}$, $\mu_1^2 \sim 1$, and $\mu_2^2 \sim 1$. Using (33) in (26)-(30), we get:

$$\frac{\partial u'^*}{\partial t^*} + \bar{u}^* \frac{\partial u'^*}{\partial x^*} + \bar{v}^* \frac{\partial u'^*}{\partial y^*} + c_{01}^* w'^* + \frac{\partial}{\partial x^*}\left(\frac{p'^*}{\bar{\rho}^*}\right) = 0, \tag{34}$$

$$\frac{\partial v'^*}{\partial t^*} + \bar{u}^* \frac{\partial v'^*}{\partial x^*} + \bar{v}^* \frac{\partial v'^*}{\partial y^*} + c_{02}^* w'^* + \frac{\partial}{\partial y^*}\left(\frac{p'^*}{\bar{\rho}^*}\right) = 0, \tag{35}$$

$$\frac{\partial w'^*}{\partial t^*} + \bar{u}^* \frac{\partial w'^*}{\partial x^*} + \bar{v}^* \frac{\partial w'^*}{\partial y^*} + \frac{\partial}{\partial z^*}\left(\frac{p'^*}{\bar{\rho}^*}\right) - \mu_2^2\left(\frac{\theta'^*}{\bar{\theta}^*}\right) = 0, \tag{36}$$

$$\frac{\partial u'^*}{\partial x^*} + \frac{\partial v'^*}{\partial y^*} + \frac{\partial w'^*}{\partial z^*} + c_{03}^* w'^* = 0, \tag{37}$$

$$\frac{\partial}{\partial t^*}\left(\frac{\theta'^*}{\bar{\theta}^*}\right) + \bar{u}^* \frac{\partial}{\partial x^*}\left(\frac{\theta'^*}{\bar{\theta}^*}\right) + \bar{v}^* \frac{\partial}{\partial y^*}\left(\frac{\theta'^*}{\bar{\theta}^*}\right) + \mu_1^2 w'^* = 0. \tag{38}$$

The small parameter used for the WKBJ expansion is $\beta = \frac{h}{L}$, where $z - z_0 = h(z^* - z_0^*)$, and $z - z_0$ is chosen such that β is on the order of 10^{-1}. We can write expansions:

$$u'^* = (u'^*)^{(0)} + \beta(u'^*)^{(1)} + \beta^2(u'^*)^{(2)} + \cdots \tag{39}$$

$$v'^* = (v'^*)^{(0)} + \beta(v'^*)^{(1)} + \beta^2(v'^*)^{(2)} + \cdots \tag{40}$$

$$w'^* = (w'^*)^{(0)} + \beta(w'^*)^{(1)} + \beta^2(w'^*)^{(2)} + \cdots \tag{41}$$

$$\frac{p'^*}{\bar{\rho}^*} = \left(\frac{p'^*}{\bar{\rho}^*}\right)^{(0)} + \beta\left(\frac{p'^*}{\bar{\rho}^*}\right)^{(1)} + \beta^2\left(\frac{p'^*}{\bar{\rho}^*}\right)^{(2)} + \cdots \tag{42}$$

$$\frac{\theta'^*}{\bar{\theta}^*} = \left(\frac{\theta'^*}{\bar{\theta}^*}\right)^{(0)} + \beta\left(\frac{\theta'^*}{\bar{\theta}^*}\right)^{(1)} + \beta^2\left(\frac{\theta'^*}{\bar{\theta}^*}\right)^{(2)} + \cdots, \tag{43}$$

where the superscipt "(0)" represents the zeroth order approximation, "(1)" the first order approximation, "(2)" the second order approximation, and so on. We also have:

$$\bar{u}^* = 1 + \beta(z^* - z_0^*), \tag{44}$$

$$\bar{v}^* = 1 + \beta(z^* - z_0^*). \tag{45}$$

Substituting (39)-(45) into (34)-(38), we find that the zeroth-order system is:

$$\frac{\partial u'^*}{\partial t^*} + u_0^*\frac{\partial u'^*}{\partial x^*} + v_0^*\frac{\partial u'^*}{\partial y^*} + c_{01}^* w'^* + \frac{\partial}{\partial x^*}\left(\frac{p'^*}{\bar{\rho}^*}\right) = 0, \tag{46}$$

$$\frac{\partial v'^*}{\partial t^*} + u_0^*\frac{\partial v'^*}{\partial x^*} + v_0^*\frac{\partial v'^*}{\partial y^*} + c_{02}^* w'^* + \frac{\partial}{\partial y^*}\left(\frac{p'^*}{\bar{\rho}^*}\right) = 0, \tag{47}$$

$$\frac{\partial w'^*}{\partial t^*} + u_0^*\frac{\partial w'^*}{\partial x^*} + v_0^*\frac{\partial w'^*}{\partial y^*} + \frac{\partial}{\partial z^*}\left(\frac{p'^*}{\bar{\rho}^*}\right) - \mu_2^2\left(\frac{\theta'^*}{\bar{\theta}^*}\right) = 0, \tag{48}$$

$$\frac{\partial u'^*}{\partial x^*} + \frac{\partial v'^*}{\partial y^*} + \frac{\partial w'^*}{\partial z^*} + c_{03}^* w'^* = 0, \tag{49}$$

$$\frac{\partial}{\partial t^*}\left(\frac{\theta'^*}{\bar{\theta}^*}\right) + u_0^* \frac{\partial}{\partial x^*}\left(\frac{\theta'^*}{\bar{\theta}^*}\right) + v_0^* \frac{\partial}{\partial y^*}\left(\frac{\theta'^*}{\bar{\theta}^*}\right) + \mu_1^2 w'^* = 0. \tag{50}$$

The dimensional form of equations (46)-(50) is:

$$\frac{\partial u'}{\partial t} + u_0 \frac{\partial u'}{\partial x} + v_0 \frac{\partial u'}{\partial y} + c_{01} w' + \frac{\partial}{\partial x}\left(\frac{p'}{\bar{\rho}}\right) = 0, \tag{51}$$

$$\frac{\partial v'}{\partial t} + u_0 \frac{\partial v'}{\partial x} + v_0 \frac{\partial v'}{\partial y} + c_{02} w' + \frac{\partial}{\partial y}\left(\frac{p'}{\bar{\rho}}\right) = 0, \tag{52}$$

$$\frac{\partial w'}{\partial t} + u_0 \frac{\partial w'}{\partial x} + v_0 \frac{\partial w'}{\partial y} + \frac{\partial}{\partial z}\left(\frac{p'}{\bar{\rho}}\right) - \frac{\theta'}{\bar{\theta}} g = 0, \tag{53}$$

$$\frac{\partial u'}{\partial x} + \frac{\partial v'}{\partial y} + \frac{\partial w'}{\partial z} + c_{03} w' = 0, \tag{54}$$

$$\frac{\partial}{\partial t}\left(\frac{\theta'}{\bar{\theta}}\right) + u_0 \frac{\partial}{\partial x}\left(\frac{\theta'}{\bar{\theta}}\right) + v_0 \frac{\partial}{\partial y}\left(\frac{\theta'}{\bar{\theta}}\right) + \frac{N_1^2}{g} w' = 0, \tag{55}$$

From the above analysis, we know that (51)-(55) apply only near the reference level, where $|z - z_0|$ is not too large, but as discussed earlier, previous studies suggest that the orientation of organized cumulus clouds can be determined in this domain. The reference level must satisfy two conditions: 1) it is unstable and 2) it has strong vertical wind shear. If we assume that the

orientation of the clouds does not change with height (this is almost always true), this set of equations can be used to meet our goal. Although we are using only the zeroth-order approximation, we know from the principles of the WKBJ method that the difference between the zeroth-order solution and the full solution is sufficiently small if the first-order terms are smaller than the zeroth-order terms.

We seek solutions of the form:

$$\begin{bmatrix} u' \\ v' \\ w' \\ p' \\ \theta' \end{bmatrix} = \begin{bmatrix} \hat{u} \\ \hat{v} \\ \hat{w} \\ \hat{p} \\ \hat{\theta} \end{bmatrix} \exp i(kx + ly + mz - \omega t)\,,\ 0 \le \quad kx', ly', mz \ \le \pi\,. \tag{56}$$

Substitute (56) into (51)-(55), After some mathematical manipulations, we find that:

$$\hat{w}\left\{\left(\frac{1}{\bar{\rho}}\frac{\partial\bar{\rho}}{\partial z} - \frac{k\dfrac{\partial\bar{u}}{\partial z} + l\dfrac{\partial\bar{v}}{\partial z}}{k\bar{u} + l\bar{v} - \omega}\right) + i\left[\frac{k^2 + l^2 + m^2}{m} - \frac{{N_1}^2(k^2 + l^2)}{m(k\bar{u} + l\bar{v} - \omega)^2}\right]\right\} = 0\,. \tag{57}$$

For nontrivial solutions:

$$\left(\frac{1}{\bar{\rho}}\frac{\partial\bar{\rho}}{\partial z} - \frac{k\dfrac{\partial\bar{u}}{\partial z} + l\dfrac{\partial\bar{v}}{\partial z}}{k\bar{u} + l\bar{v} - \omega}\right) + i\left[\frac{k^2 + l^2 + m^2}{m} - \frac{N_1^2(k^2 + l^2)}{m(k\bar{u} + l\bar{v} - \omega)^2}\right] = 0\,. \tag{58}$$

We distinguish two types of solutions:

Type I: ω is real. From (58) we obtain:

$$N_1^2 = \frac{k^2 + l^2 + m^2}{k^2 + l^2}(k\bar{u} + l\bar{v} - \omega)^2, \tag{59}$$

$$\frac{1}{\bar{\rho}}\frac{\partial \bar{\rho}}{\partial z} - \frac{k\frac{\partial \bar{u}}{\partial z} + l\frac{\partial \bar{v}}{\partial z}}{k\bar{u} + l\bar{v} - \omega} = 0. \tag{60}$$

From (59), we see that N_1^2 is greater than or equal to 0. For thermal instability to occur, N_1^2 must always less than 0 before the cumulus processes begin. The cumulus processes can not make N_1^2 too much greater than 0, because otherwise the convection will stop. Before the convection begins, N_1^2 can not be much less than 0, because otherwise $N_1^2 < 0$ will continue for some time. For these reasons, we expect that $N_1^2 \approx 0$ in this case. This is consistent with our assumption that ω is real. From (59), we conclude that

$$k\bar{u} + l\bar{v} - \omega \approx 0. \tag{61}$$

Using $\omega = c\sqrt{k^2 + l^2}$, we can calculate the phase speed of the organized clouds:

$$c \approx \frac{ku_0 + lv_0}{\sqrt{k^2 + l^2}}. \tag{62}$$

From (62), we see that the phase speed is approximately determined by the environmental wind and the organization of the clouds. Because $k\bar{u} + l\bar{v} - \omega \approx 0$, we see that for (60) to be satisfied, we need $k\frac{\partial \bar{u}}{\partial z} + l\frac{\partial \bar{v}}{\partial z} \approx 0$. Using $L_x = \frac{2\pi}{k}, \quad L_y = \frac{2\pi}{l}$, we obtain

$$\frac{L_x}{L_y} \approx \left| \frac{\frac{\partial \bar{u}}{\partial z}}{\frac{\partial \bar{v}}{\partial z}} \right| . \tag{63}$$

In case $\left|\frac{\partial \bar{u}}{\partial z}\right| \gg \left|\frac{\partial \bar{v}}{\partial z}\right|$ ($\left|\frac{\partial \bar{u}}{\partial z}\right| \ll \left|\frac{\partial \bar{v}}{\partial z}\right|$), $L_x \gg L_y (L_x \ll L_y)$. What this means is that the wind shear is parallel to the line. For $\left|\frac{\partial \bar{u}}{\partial z}\right| \sim \left|\frac{\partial \bar{v}}{\partial z}\right|$, we have a nonlinear MCS.

Type II: ω is complex. In this case, the convection is growing, so we expect that N_1^2 is less than 0. From (58), we find that:

$$\left[\frac{m}{\bar{\rho}}\frac{\partial \bar{\rho}}{\partial z} + (k^2 + l^2 + m^2)i\right](k\bar{u} + l\bar{v} - \omega)^2 - m\left(k\frac{\partial \bar{u}}{\partial z} + l\frac{\partial \bar{v}}{\partial z}\right)(k\bar{u} + l\bar{v} - \omega) - iN_1{}^2(k^2 + l^2) = 0 . \tag{64}$$

Because $\frac{m}{\bar{\rho}}\frac{\partial \bar{\rho}}{\partial z} \sim 6.28 \times 10^{-8}\,\mathrm{m}^{-2}$ and $(k^2 + l^2 + m^2) \sim 1.18 \times 10^{-6}\,\mathrm{m}^{-2}$, we can neglect $\frac{m}{\bar{\rho}}\frac{\partial \bar{\rho}}{\partial z}$ in (64):

$$(k^2 + l^2 + m^2)i(k\bar{u} + l\bar{v} - \omega)^2 - m\left(k\frac{\partial \bar{u}}{\partial z} + l\frac{\partial \bar{v}}{\partial z}\right)(k\bar{u} + l\bar{v} - \omega) - iN_1{}^2(k^2 + l^2) \approx 0 . \tag{65}$$

Setting $\omega = \omega_r + \omega_i i$, and solving (65), we obtain:

$$\omega_r = k u_0 + l v_0, \tag{66}$$

$$\omega_i = \frac{m\left(k\frac{\partial \bar{u}}{\partial z} + l\frac{\partial \bar{v}}{\partial z}\right) + \sqrt{m^2\left(k\frac{\partial \bar{u}}{\partial z} + l\frac{\partial \bar{v}}{\partial z}\right)^2 - 4N_1^2(k^2+l^2)(k^2+l^2+m^2)}}{2(k^2+l^2+m^2)}, \tag{67}$$

where the decaying solution has been discarded. From (66), we get the same phase-speed formula as for Type I, i. e. (62). The most rapid growth rate occurs for

$$\frac{\partial \omega_i}{\partial k} = 0, \text{ and} \tag{68}$$

$$\frac{\partial \omega_i}{\partial l} = 0. \tag{69}$$

Substituting (67) into (68) and (69), and letting $a \equiv m\left(k\frac{\partial \bar{u}}{\partial z} + l\frac{\partial \bar{v}}{\partial z}\right)$ and $b^2 \equiv k^2 + l^2 + m^2$, we get

$$\left[a + \sqrt{a^2 - 4N_1^2 b^2(b^2 - m^2)}\right]\left(m\frac{\partial \bar{u}}{\partial z}b - 2ka\right) = 4kN_1^2 m^2 b, \tag{70}$$

$$\left[a + \sqrt{a^2 - 4N_1^2 b^2(b^2 - m^2)}\right]\left(m\frac{\partial \bar{v}}{\partial z}b - 2la\right) = 4lN_1^2 m^2 b. \tag{71}$$

From the ratio of (70) to (71), we find that $l\frac{\partial \bar{u}}{\partial z} = k\frac{\partial \bar{v}}{\partial z}$, so we have

$$\frac{L_x}{L_y} = \left|\frac{\frac{\partial \bar{v}}{\partial z}}{\frac{\partial \bar{u}}{\partial z}}\right|. \tag{72}$$

In case $\left|\frac{\partial \bar{u}}{\partial z}\right| \gg \left|\frac{\partial \bar{v}}{\partial z}\right|$ ($\left|\frac{\partial \bar{u}}{\partial z}\right| \ll \left|\frac{\partial \bar{v}}{\partial z}\right|$), $L_x \ll L_y (L_x \gg L_y)$. What this means is that the vertical wind shear is perpendicular to the line. For $\left|\frac{\partial \bar{u}}{\partial z}\right| \sim \left|\frac{\partial \bar{v}}{\partial z}\right|$, we have a nonlinear MCS.

Now we have derived conditions to determine the aspect ratio of the organized cloud system: formula (63), which applies when N_1^2 is close to zero; and formula (72), which applies when N_1^2 is less than zero. We choose

$$(N_1^2)_{critical} = -5 \times 10^{-5}\ \mathrm{s}^{-2} \tag{73}$$

as the threshold value to distinguish these two cases. Tests show that this value works well for GATE, ARM (the Southern Great Plains Site of the Atmospheric Radiation Measurements Project) EMEX, SCSMEX, and TOGA COARE data. However, more experiments are needed for a better determination of this criterion. For N_1^2 close to the critical value, the mesoscale system is regarded as a nonlinear MCS or a linear MCS with no preferred orientation (Lemone et al. 1998).

Before continuing the discussion of the orientation of the organized cumulus clouds, we test the theory by applying it to the fast-movers and slow-movers reported by Barnes and Sieckman (1984; all data is available in *Mon. Wea. Rev.*, **112**, 1782-1794). We choose the reference level to be 3 km above the cloud base for two reasons: 1) the two conditions for reference level are satisfied in this level for both the fast movers and slow movers, and 2) the horizontal velocity components at this level are the mean value of all the levels satisfying the two conditions.

For the fast movers, we find that $N_1^2 = -9.3\times10^{-5}\ \mathrm{s}^{-2}$ as calculated by (31), so this is a Type II case. From (72) $\dfrac{L_P}{L_N} = \left|\dfrac{\dfrac{\partial \bar{v}_N}{\partial z}}{\dfrac{\partial \bar{v}_P}{\partial z}}\right| = 16.1$, where the subscripts P and N refer to variables parallel and normal to the line, respectively. $\bar{v}_N$ and $\bar{v}_P$ are calculated using a linear fit to the low level wind. Because the ratio of the two wave lengths is greater than 10, we interpret this case as a squall line. These ratio is calculate from a composite vertical wind shear from three soundings. We do not know the observed aspect ratio, however, this number is realistic for a common squall line. This is a Type II case. The orientation of the squall line is perpendicular to the vertical wind shear. Using (62), we estimate that the phase speed of the squall line was about -12 m s^{-1}. This compares well with the observed speed of -11.1 m s^{-1}.

For the slow movers, $N_1^2 = -1.86\times10^{-5}(\ s^{-2})$, so this is a Type I case. From (63), we find that $\frac{L_P}{L_N} = \left|\frac{\frac{\partial \bar{v}_P}{\partial z}}{\frac{\partial \bar{v}_N}{\partial z}}\right| = 12.5$. Again, we regard this as a squall line. Using (62), we estimate that the phase speed of the squall line is -2 m s^{-1}. The observed speed was about -2.2 m s^{-1}.

An additional condition is needed to determine the horizontal dimensions of the organized clouds. If the shape of the cloud system is an ellipse, the area is

$$\sigma = \frac{1}{4}\pi L_x L_y . \tag{74}$$

By combining (63) or (72) with (74), we can determine L_x and L_y for the organized cumulus clouds, if the area is known. We assume that the area of the mesoscale region is one order of magnitude larger than the collective area of the convective updrafts. A method to determine the updraft area is described later.

The vertical wave number of the organized clouds, m, can be calculated from the lower and upper boundary conditions:

$$w'(z=z_B) = 0, \tag{75}$$

$$w'(z=z_T) = 0. \tag{76}$$

Here z_T is the highest cloud-top height, and z_B is the lowest cloud-base height of the elliptical system. Substitute (56) into (75) and (76):

$$m = \frac{\pi}{z_T - z_B}. \tag{77}$$

We also need to determine the angle between the linear MCS and the axis. A linear MCS is defined to be oriented such that it has a maximum or minimum $\frac{L_x}{L_y}$. For example, fast movers orientated such that one of its axis is as large as possible and the other one is as small as possible from (72). If we rotate the coordinate, the length of the two wave lengths will not have such big difference. The condition for a linear MCS is:

$$\left|\frac{L_x}{L_y}\right| < 0.1 \quad \text{or} \quad \left|\frac{L_x}{L_y}\right| > 10. \tag{78}$$

Only one of these conditions can be satisfied.

In summary, we first choose a reference level using the two conditions (for deep clouds, about 2-4 kilometers above cloud base; for shallow clouds, at lower level). Using (73), we distinguish Type I from Type II (Table 1). Then a linear fit is used to calculate the low-level wind shear. We calculate the aspect ratio using (63) or (72) with (74), and distinguish between linear MCSs and nonlinear MCSs using (78). Finally, (62) is used to calculate the phase speed of the convective system.

Our approach is consistent with the previous work, and also represents some progress. We use the thermodynamic condition (73) to distinguish the two cases: a line normal to the vertical wind shear and a line parallel to the vertical wind shear. The vertical wind shear is used to determine the aspect ratio of the line. We have also given a method to determine the orientation and the phase speed.

The preferred convectively growing modes reported by Asai (1970, 1972), including both thermal and inertial instability, belong to our Type I. In his experiments, N_1^2 is larger than $-5 \times 10^{-5}\ \mathrm{s}^{-2}$.

Our theory can explain the orientation, aspect ratio and phase speed of the GATE fast-movers and slow-movers.

Our theory is consistent with the mechanism proposed by Rotunno et al. 1988, which applies for large $\left|N_1^2\right|$. Strong downdrafts are associated with large growth rates and CAPE, and smaller θ_e in the upper levels causes stronger cold pool. So the balance between the large low-level shear and the cold pool determines the orientation of the line.

These formulae apply not only for the whole troposphere, but also for any level of the troposphere. Both low-level shear and $\left|N_1^2\right|$ (see Alexander and Young, 1992 and Lemon et al. 1998) tend to be large in many cases, so shear-normal linear MCSs of Type II tend to develop for

large low-level wind shear. However, large middle-level shear is often associated with small $\left|N_1^2\right|$, so Type I linear MCSs tend to develop. This is why shear-parallel linear MCSs tend to develop for large middle-level wind shear. When both the low-level and middle-shear are large, Type I linear MCSs tend to develop. This is what Alexander and Young (1992), Lemon et al. (1998) and Johnson and Keenan (2001) found. Johnson and Keenan (2001) found a special case on May 23, 1998, in which the low-level shear is parallel to the orientation of the linear MCS. We checked the soundings for this case. $\left|N_1^2\right| = -5\times10^{-6}\ \mathrm{s}^{-2}$ at the reference level (1000 m - 2000 m), which is much smaller than the critical value. This case can be well explained by our theory. It belongs to Type I.

From earlier studies we know that the low-level wind is very important for the orientation of organized clouds. This can be explained by our theory, because the wind shear distribution that we assumed is most likely to occur in the low and unstable levels.

3. Modification of the environmental flow by cumulus clouds

From above analysis, we can calculate the orientation, aspect ratio and phase speed of the organized mesoscale system. For this theory to be used in a cumulus parameterization, we need to assume that every cloud type inside the grid box has the same orientation and aspect ratio as the mesoscale system itself. This assumption was used by Wu and Yanai (1994), whose results compared well with observations.

The pressure-gradient force equation (1) can be used for the individual cumulus clouds. The vertical velocity profile for the cumulus clouds is assumed to be approximately bell shaped. However, the magnitude of the cumulus vertical velocity is larger than that of the mesoscale system. So substituting (3), (4), (5) and (7) into the terms on the right-hand side of (1), we get perturbation pressure-gradient forces for individual cumulus clouds given by (15), (19), (23), (24) and (25).

For one type of cloud at a given level, the large-scale effect of momentum transported by cumulus clouds is represented by

$$\frac{d}{dt}\bar{\boldsymbol{v}} = \boldsymbol{F}_c = -\frac{1}{\rho}\frac{\partial}{\partial z}(\rho\overline{\boldsymbol{v}'w'}) = -\frac{1}{\rho}\frac{\partial}{\partial z}[M_c(\boldsymbol{v}_c - \bar{\boldsymbol{v}})] \quad , \tag{79}$$

where $M_c = \rho_c \sigma_c w_c$ is the vertical mass flux associated with the cumulus clouds; σ_c is the fractional area covered by the cumulus updrafts; $\boldsymbol{v}_c$ and $\bar{\boldsymbol{v}}$ are the updraft-mean velocity and the large scale wind. $\boldsymbol{F}_c$ was first used in a GCM by Arakawa et al. (1972) and was called “cumulus friction” by Schneider and Lindzen (1976). Here we show only one cloud type. Actually many cloud types are allowed in our model.

Following Shapiro and Stevens (1980) and Wu and Yanai (1994):

$$\boldsymbol{F}_c = D_c(\boldsymbol{V} - \bar{\boldsymbol{V}}) + M_c\frac{\partial \bar{\boldsymbol{v}}}{\partial z} + \sigma_c\frac{1}{\rho}\nabla p_c \,. \tag{80}$$

The first term on the right-hand side of (80) represents the detrainment of momentum from the cumulus clouds to the environment. The second term represents vertical advection by the environmental subsidence induced by the cumulus clouds. The third term represents the cloud-scale perturbation pressure-gradient force. Because the detrainment rate and the cloud mass flux can be determined in terms of the large-scale variables (Arakawa and Schubert 1974), the momentum flux parameterization is reduced to determining the horizontal velocity of the detrained air and the convective-scale pressure-gradient force.

4. Data and experiment design

The CSU SCM (single column model) is used in this study to investigate the new scheme and convective momentum transport. The model has 17 levels. We have used “revealed” forcing. More details of the model are given by Randall and Cripe (1999).

Two kinds of simulations have been performed. The simulations started from the same initial time (17:30 June 18, 1997) and ran for 30 days. The first kind of simulation (designated as MR) employs the new cumulus momentum transport parameterization introduced here. In the second kind of simulation (the control run, CR), the contribution of the perturbation pressure-gradient force is neglected. One objective of these simulations is to test the orientation, aspect ratio and phase speed of organized convections predicted by the theory. Another objective is to find the frictional force due to the momentum flux associated with the cumulus convection. Comparison of the MR and CR runs will show how much the perturbation pressure-gradient force contributes to the vertical momentum transport.

ARM data is used to drive the SCM and provides the initial conditions. We also use other ARM data for the same period to evaluate the two simulations. There are 12 observing stations that supply the data for the SCM. The center of the box is at 97.49°W and 36.61°N. For more details, see Randall and Cripe (1999).

5. Results of numerical simulations

In this section, we present the results of the new parameterization. We will show how the convective-scale pressure-gradient force, produced by the interaction of vertical wind shear with organized convection, influences the simulated momentum flux.

Let us first see what kind of convective processes occurred during this period. ***Fig. 2*** shows the observed total rain. There are about six precipitation events. We have radar data only from June 18 to June 27, June 30 to July 4, July 9 to July 11 and July 13 to July 15. The stronger events occurred during June 26 and can be seen in the radar data. Both nonlinear and linear MCS can be seen on June 26.

5.1 The orientation of the convection

During this integration period, there are several ways in which we can test our theory of organized convections. We choose some cases which can represent the characteristics of the linear MCSs and nonlinear MCSs.

Fig. 3(a) shows the predicted orientation for July 15 12:15,1997 (Case 1). ***Fig. 3*** (b) shows the corresponding observed orientation of the squall line. The mesoscale area is calculated by increasing the collective convective cloud area by 8 times:

$$\sigma_s = 8\sum_i \sigma_{ci}. \tag{81}$$

Here σ_s is the area of the mesoscale system and σ_{ci} is the area of the cumulus cloud type i. σ_{ci} is calculated by:

$$\sigma_{ci} = \frac{M_{ci}}{\rho w_{ci}}. \tag{82}$$

w_{ci} can be calculated by the vertical momentum budget of the updraft (Simpson and Wiggert 1969, Cheng 1989):

$$w_{ci}^{\ 2} = -\frac{g\left[\dfrac{\overline{T}_{vi} - T_{ci}}{\overline{T}_{vi}} + l_{ci} + q_{ri}\right]}{f_1(1+\gamma)\left[2\lambda - \dfrac{1}{\rho_{ci}}\dfrac{\partial \rho_{ci}}{\partial z}\right]}, \tag{83}$$

where T is the temperature, l_c is the liquid water content of cloud, q_{ri} is the rainwater mixing ratio, f_1 is a constant, γ is the virtual mass coefficient, λ is the entrainment rate, and ρ_{ci} is the density of the cloud air. The mass flux M_{ci} is calculated by using prognostic closure (Pan and

Randall 1998) with the CKE (Convective Kinetic Energy) equation. The scale of the convective ellipse is about $11.1 \text{ km} \times 148 \text{ km}$. Because an extremely complex iteration is needed to calculate the vertical perturbation pressure-gradient force, we do not use the formulae that we derived to calculate the vertical velocity here. This is a simple case. Only one squall line existed in the box. The orientation of the squall line is close to north-south. The vertical wind shear in the unstable levels satisfies $\frac{L_y}{L_x} = \left| \frac{\frac{\partial \bar{v}_y}{\partial z}}{\frac{\partial \bar{v}_x}{\partial z}} \right| \gg 1$. This is a case which the vertical wind shear is parallel to the line. From our theory the phase speed is about 1.9 m s^{-1} normal to the squall line and about -0.3 m s^{-1} parallel to the line. We have estimated the line velocity from radar-data animations. The predicted orientation and speed are in good agreement with the observations.

Fig. 4 (a) shows the orientation of the squall line as seen by radar on June 26, 14:30, 1997 (case 2). ***Fig. 4*** (b) shows the orientation from the theory for that time. The scale of the convective ellipse is about $10 \text{ km} \times 132 \text{ km}$. The orientations from the theory and the observations agree very well. Both lie in north-east to south-west direction. From theory, the phase speed normal to the squall line is 6.7 m s^{-1}, and parallel to the line is 0.1 m s^{-1}. Compared to the radar data, the line's speed and direction are approximately right.

The last case (Case 3) is a nonlinear MCS case. ***Fig. 5*** (a) shows the organized clouds as observed by radar on June 26, 8:45 AM, 1997. ***Fig. 5*** (b) shows the clouds as predicted by the theory. The scale of the convective circle is about $57 \text{ km} \times 57 \text{ km}$. This is a very complex case.

The left lobe and the right lobe of the cloud system are nonlinear MCSs. There is a small rain band lying in the north-east to south-west direction, which looks like a linear MCS in the center of the box. However, all of the clouds in the box are nonlinear MCSs according to the theory. Actually Case 3 occurred first, the organized clouds gradually became a weak linear MCS (Case 2) in the afternoon. The phase speed from the model is 4 m s^{-1} in west-east direction, -0.7 m s^{-1} in south-north direction according to our theory. Compared to the radar data, the direction and speed are approximately right.

5.2 The vertical momentum transport due to cumulus convection

5.2.1 Nonlinear MCS case

The vertical transport of the horizontal momentum by nonlinear MCSs is very important because most of the organized clouds tend to be of this type. ***Fig. 6*** shows the u and v wind components and their tendencies for the nonlinear MCS on June 26, 8:45 AM (Case 3). Comparing the result from the MR and CR runs, we find that the effects of the perturbation pressure-gradient force tend to cancel the combined effects of detrainment and environmental subsidence in both directions. The effects of the perturbation pressure-gradient force are upgradient in the upper levels. This can be explained by (24) and (25) with $\theta = 0$:

$$-\sigma_c\left(\frac{1}{\rho}\cdot\frac{\partial p'}{\partial x}\right) = \frac{\nu_k}{\rho}\cdot\frac{\partial \bar{u}}{\partial z}M_c, \tag{84}$$

$$-\sigma_c\left(\frac{1}{\rho}\cdot\frac{\partial p'}{\partial y}\right) = \frac{\nu_l}{\rho}\cdot\frac{\partial \bar{v}}{\partial z}M_c. \tag{85}$$

The pressure-gradient force is positively proportional to the vertical wind shear because ν_k, ν_l and M_c are all positive. In the upper layer, the vertical wind shear is larger, so the acceleration is larger. The total transport is upgradient in both directions. We can see that the tendencies tend to eliminate the vertical wind shear. For example, the u momentum tends to decrease in the upper levels and increase in the lower levels. This can be explained when (84) and (85) are substituted into (80):

$$F_x = D_{cx}(u_{cx} - \bar{u}) + M_c \frac{\partial \bar{u}}{\partial z}(1 - \nu_x), \tag{86}$$

$$F_y = D_{cy}(v_{cy} - \bar{v}) + M_c \frac{\partial \bar{v}}{\partial z}(1 - \nu_y). \tag{87}$$

Because ν_x and ν_y are less than 1, u monotonically increases in z the direction, and v increases with z to about 600 mb, the contributions of the last two terms of (86) and (87) are positive. In the entrainment levels (low levels, where $D_{cx} \approx 0$ and $D_{cy} \approx 0$), the air in the environment is accelerated; the air in the updraft is decelerated. In the detrainment-levels, the velocity of the air in the updraft is less than that of the environmental air, so the detrainment of the low-momentum air in the upper layer will decrease the shear (Wu and Yanai, 1994). If u decreases and then increases below the jet level, then the horizontal velocity of the air in the updraft can be larger than the environmental velocity. The detrainment of the higher momentum air will increase the

shear. From (86) and (87), we also can see that the effects of the perturbation pressure-gradient force and vertical advection tend to cancel with each other, because ν_x and ν_y are always positive. For this case, vertical advection is dominant.

5.2.2 Linear MCS case

We investigate two kinds of linear MCS cases here. In Case 1, the line lies along the y axis, and in Case 2, the line makes an angle with the y axis. ***Fig. 7*** shows the u and v wind components and their tendencies for the linear MCS on July 15, 12:15 (Case 1). Comparing the MR and CR runs, we find that the perturbation pressure-gradient force has almost no effect in the line-parallel direction (y direction), but has a strong effect in the line-normal direction (x direction). In the line-normal direction, the upgradient transport is caused mainly by the perturbation pressure-gradient force. The effects of both detrainment and environmental subsidence are downgradient in the line-normal direction. This is obvious from (86) and (87). In this case, $\nu_x \gg 1$ and $\nu_y \ll 1$, so the perturbation gradient force has a big effect in the x direction and almost no effect in the y direction. The upgradient momentum transport in the upper levels by the perturbation pressure-gradient force in the x direction is due to the same reason given before. The total transport (blue line) is downgradient in the y direction and upgradient in the x direction. Using (86) and (87), we find that the u momentum below the detrainment level is greater than that of the environment and v momentum is less than that of the environment, so detrainment will tend to strengthen the wind shear in the u direction and weaken the wind shear in the v direction at the upper levels.

Fig. 8 shows the u and v winds and their tendencies for the linear MCS on June 26, 14:30 (Case 2). The line makes a small angle with the y direction. In the y direction, the total transport is downgradient. The perturbation pressure-gradient force tends to re-enforce the effects of the other two effects in the upper layer and to cancel the other two effects in the middle and lower layer. In the x direction, the total effect is to increase the wind in the upper layer and decrease the wind in the lower layer. The perturbation pressure-gradient force is the main factor causing the upgradient transport.

In summary, the vertical momentum transport associated with the perturbation pressure-gradient force tends to be upgradient in both directions for nonlinear MCSs, and in the line-normal direction for linear MCSs. This is consistent with the conclusions of Moncrieff (1992) and Wu and Yanai (1994).

The total momentum transport is downgradient in both directions for the nonlinear MCSs Stevens 1979, Tollerud and Esbensen 1983, Lemone et al. 1984, and Sui and Yanai 1986 reported downgradient convective momentum transport for nonlinear MCSs. For linear MCSs, the total momentum transport tends to be upgradient in the line-normal direction. Moncrieff and Green 1972, Tollerud and Esbensen 1983, Lafore et al. 1988, LeMone and Jorgensen 1991, and Gallus and Johnson 1992 reported upgradient momentum transport associated with cumulus clouds for this case. It tends to be downgradient in the line-parallel direction. These results are consistent with the studies of Asai (1970), Lemone and Jorgensen (1991) and Wu and Yanai (1994).

The effects of the perturbation pressure-gradient force and the other effects tend to cancel with each other. This result is consistent with the study of Wu and Yanai (1994).

6. Summary and discussion

In this study, a parameterization of cumulus momentum transport has been proposed. An important feature of this scheme is the inclusion of the perturbation pressure-gradient force induced by interactions between the updraft and the environmental wind. Another important feature is that the orientation, aspect ratio, and phase speed of organized convection are determined.

By comparing the predicted orientation, aspect ratio and phase speed of organized convection with those observed by radar, we find that our theory gives the right answers. According to our theory, the orientation of a squall line can make any angle with the vertical wind shear.

The effects of convective-scale momentum transport have also been studied. The vertical momentum redistribution is systematically different between linear and nonlinear MCSs. For non-linear MCSs, the total momentum transport tends to be downgradient, but one of the two components (u or v) can be upgradient if the environmental wind profile has a certain shape. For linear MCSs, line-normal vertical momentum transport tends to be upgradient, while line-parallel transport tends to be downgradient.

The momentum transport due to the perturbation pressure-gradient force has effects not only at higher levels, but also at lower levels. It tends to make the transport upgradient and tends to cancel with vertical momentum advection and detrainment effects.

Compared with Wu and Yanai's (1994) scheme, our scheme is more complete because we have figured out a way to calculate the orientation of the organized cumulus clouds. In addition, our theory of the perturbation pressure-gradient force extends that of Wu and Yanai. The organized cumulus clouds in our theory are seen as entities embedded inside a mesoscale system, so the momentum transport mechanism of the cumulus clouds is easy to understand. We also consider the nonlinear effects on the perturbation pressure-gradient force, which are significant in the vertical direction. Further discussion will be given elsewhere.

Our theory can easily be subjected to tests using observations. Although we have used GATE, ARM, EMEX, SCSMEX, and TOGA COARE cases to test the theory, more tests are necessary. Our criterion to distinguish line parallel and line normal linear MCSs is the instability near reference level. A reference level must satisfy two conditions. Even weak instability at the reference level, there can be strong instability in the other layers, so the CAPE and growth rate for Type I can still be larger. That is the reason why we can not distinguish Type I and Type II using CAPE and growth rate as criteria. CAPE and growth rate must be pretty large for Type II MCSs, but they are not necessary small for Type I.

Using the methods described above, we can obtain the velocity of convective system, which is important for the physical processes in GCMs. For example, a convective system with a small speed tends to produce heavy local rain and long-lasting local cloud.

Our scheme also diagnostically determines the vertical velocity of the updraft air, which is important for the parameterizations of the microphysical processes inside cumulus clouds.

However, many important, interesting and challenging questions remain. What are the effects of the downdrafts and the mesoscale system on the vertical momentum transport? What is the relationship between the vertical momentum transport by the updraft, downdraft and the mesoscale system? These are two questions that we will answer in our future work.

Acknowledgements

This study has been supported by National Science Foundation under grant ATM-9812384 and by the U.S. Department of Energy's ARM Program under grant DE-FG03-95ER61968. The ARM data was kindly provided by Douglas G. Cripe of Colorado State University, Mike Splitt of the University of Utah, Minghua Zhang of State University of New York at Stony Brook, and Richard Cederwall of Lawrence Livermore National Laboratory. The authors also benefitted from discussions with Professors R. Johnson and W. Schubert of Colorado State University.

References

Alexander, G. D., and G. S. Young, 1992: The relationship between EMEX mesoscale

precipitation feature properties and their environmental characteristics. *Mon. Wea. Rev.*, **120**, 554-564.

Arakawa, A., and W. H. Schubert, 1974: The interaction of a cumulus cloud ensemble with the large-scale environment, Part I. *J. Atmos. Sci.*,**31**,674-701.

----------, Y. Mintz, A. Katayama, J. -W. Kim, W. Schubert, T. Tokioka, M. Schlesinger, W. Chao, D. A. Randall and S. Lord, 1972: The UCLA atmospheric General Circulation Model, *Notes Distributed at the workshop*, 25 March - 4 April 1974, Department of Meteorology, University of California, Los Angeles, California 90024.

Asai, T., 1970: Three-dimensional features of thermal convection in a plane Couette flow. *J. Meteor. Soc. Japan*, **48**, 18-29.

Asai, T., 1970: Stability of a plane parallell flow with variable vertical shear and unstable stratification. *J. Meteor. Soc. Japan*, **48**, 129-138.

Asai, T., 1972: Thermal instability of a shear flow turning the direction with height. *J. Meteor. Soc. Japan*, **50**, 525-531.

Barnes, G.M., and K. Sieckman, 1984: The environment of fast- and slow-moving tropical mesoscale convective cloud lines. *Mon. Wea. Rev.*, **112**, 1782-1794.

Betts, A.K., 1976: The thermodynamic transformation of the tropical subcloud layer by precipitation and downdrafts. *J.Atmos.Sci.*, **33**, 1008-1020.

Bluestein, H.B., and M.H. Jain, 1985: Formation of mesoscale lines of precipitation: Severe

squall lines in Oklahoma during the spring. *J.Atmos.Sci*.,**42**,1711-1732.

----------, G.T. Marx and M.H. Jain, 1987: Formation of mesoscale lines of precipitation: Non-severe squall lines in Oklahoma during the spring. *Mon. Wea. Rev.*, **115**,2719-2727.

Cheng, M.-D., 1989a: Effects of downdrafts and mesoscale convective organization on the heat and moisture budgets of tropical cloud cluster. Part I: A diagnostic cumulus ensemble model. *J. Atoms. Sci.*,**46**,1517-1538.

-------, -------, A. Arakawa, 1997: Inclusion of rainwater budget and convective downdrafts in the Arakawa-Schubert cumulus parameterization. *J. Atoms. Sci*., **54**, 1359-1379.

Ding, P., and D. A. Randall, 1998: A cumulus parameterization with multiple cloud-base levels. *J. Geophys. Res*.,**103**,11341-11354.

Frank, W.M.,1978: The life cycle of GATE convective systems. *J.Atmos.Sci.*, **35**,1256-1264.

Gallus, W. A., Jr., and R. H. Johnson, 1992: The momentum budget of an intense midlatitude squall line. *J. Atmos. Sci.*, **49**, 422-450.

Hane, C., E., and P. S. Ray, 1985: Pressure and buoyancy fields derived from Doppler radar data in a tornadic thunderstorm. *J. Atmos. Sci*., **42**, 18-35.

Holton, J.R., 1973: A one-dimensional cumulus model including pressure perturbations. *Mon. Wea. Rev.*, **101**, 201-205.

Johnson, R.H., and P. J. Hamilton, 1988: The relationship of surface pressure features to the precipitation and airflow structure of an intense midlatitude squall line. *Mon. Wea. Rev.*,

116,1444-1472.

----------, and T.D. Keenan, 2001: Organization of oceanic convection during the onset of the 1998 East Asian summer monsoon. *Preprints, 30th International Conference on Radar Meteorology, Amer. Meteor. Soc.*, Munich, Germany.

Jorgensen, D. P., M. A, LeMone, and *B.* J.-D. Jou, 1991: Precipitation and kinematic structure Of an Oceanic mesoscale convective system. Part 1: Convective line structure. *Mon. Wea. Rev.,* **119**, *2*608-2637.

Lafore, J.-P., J-L. Redelsperger, and G. Jaubert, 1988: Comparison between a three-dimensional simulation and Doppler radar data of a tropical squall line: Transports of mass, momentum and moisture. *J. Atmos. Sci.,* **45**, 3483-3500.

Lemone, M. A., and M. W. Moncrieff, 1994: Momentum and mass transport by convective bands: Comparisons of highly idealized dynamic models to observations. *J. Atmos. Sci*., **51**, 281-305.

----------, and D. P. Jorgensen, 1991: Precipitation and kinematic structure of an oceanic mesoscale convective system. Part 11: Momentum transport and generation. *Mon. Wea. Rev.,* **119**, 2639-2653.

----------, G. M. Barnes, and E. J. Zipser, 1984: Momentum flux by lines of cumulonimbus over the tropical oceans. *J. Atmos. Sci.*, **41**,1914-1932.

----------, G. M. Barnes, J.C. Fankhauser, and L. F. Tarleton, 1988: Perturbation pressure fields measured by aircraft around the cloud base updraft of deep convective clouds. *Mon.*

Wea. Rev., **116**, 313-327.

----------, E. J. Zipser and S. B. Trier,1998: The role of environmental shear and thermodynamic conditions in determining the structure and evolution of mesoscale convective systems during TOGA COARE. *J. Atmos. Sci.*, **55**, 3493-3518.

Lin, Y. J., T. C., Wang, and J. H. Lin, 1986: Pressure and temperature perturbations within a squall line thunderstorm derived from SESAME dual-Doppler data. *J. Atmos. Sci.*, **43**, 2302-2327.

Lilly, D.K., 1979: The dynamic structure and evolution of thunderstorms and squall lines. *Ann. Rev. Earth planet. Sci.*, **7**, 117-171

Ludlam, F. H.,1963: Severe local storms: a review. *Meteor. Monogr.*, **5**, Amer. Meteor. Soc. 1-30.

----------, 1980: *Clouds and Storms*. Pennsylvania State University Press, 404p.

Moncrieff, M. W., and J. S. A. Green, 1972: The propagation and transfer properties of steady convective overturning in shear. *Quart. J. Roy. Meteor. Soc.*, **98**, 336-352.

----------, 1992: organized convective systems: Archetypal dynamical models, mass and momentum flux theory, and parameterization. *Quart. J. Roy. Meteor. Soc.*, **107**,29-50.

Newton, C.W., 1966: Circulations in large sheared cumulonimbus. *Tellus*, **18**, 699-713

Ogura, Y., and N. A. Phillips, 1962: A scale analysis of deep and shallow convection in the atmosphere. *J. Atmos. Sci*., **30**, 1276-1286.

Pan, D.-M., and D. A. Randall, 1998: A cumulus parameterization with a prognostic closure.

Quart.J.Roy.Meteor.Soc.,**124**,949-981.

Randall, D. A., K.-M. Xu, R. J. C. Somerville, and S. Iacobellis, 1996: Single-column models and cloud ensemble models as links between observations and climate models. *J. Climate*, **9**, 1683-1697.

Randall, D. A. and D. G. Cripe, 1999: Alternative methods for specification of observed forcing in single-column models and cloud system models, *J. Geophys*, **104**, 24,527-24,545.

Rotunno, R., and J. B. Klemp,1982: The influence of the shear-induced pressure gradient on the thunderstorm motion. *Mon. Wea. Rev.*, **110**,136-151.

----------,----------, and M. L. Weisman, 1988: A theory for strong, long-lived squall lines. *J. Atmos. Sci.,* **45**,463-485

Schneider, E. K., and R. S. Lindzen, 1976: A discussion of the parameterization of momentum exchange by cumulus convection. *J. Geophys. Res*., **81**,3158-3160.

Seitter, K. L., and H.-L. Kuo,1983: The dynamical structure of squall-line type thunderstorms. *J. Atmos. Sci*., **40**, 2832-2854.

Shapiro, L. J., and D. E. Stevens, 1980: Parameterization Of convective effects on the momentum and vorticity budgets of synoptic-scale Atlantic tropical waves. *Mon. Wea. Rev.,* **108,** 1816-1826.

Simpson, J., and V. Wiggert, 1969: Models of precipitating cumulus towers. *Mon. Wea. Rev.*, **97**, 471-489.

Soong, S.-T., and W.-K. Tao, 1984: A numerical study of the vertical transport of momentum in a

tropical rainband. *J. Atmos. Sci.,* **41**, 1049-1061.

Stevens, D. E., 1979: Vorticity, momentum and divergence budgets of synoptic-scale wave disturbances in the tropical eastern Atlantic. *Mon. Wea. Rev.*, **107**, 535-550.

Sui, C.-H., and M., Yanai, 1986: Cumulus ensemble effects on the large-scale vorticity and momentum fields of GATE. Part 1: Observational evidence. *J. Atmos. Sci.*, **43**,1618-1642.

--------, and M.-D. Cheng, X. Wu, and M. Yanai, 1989: Cumulus ensemble effects on the large-scale vorticity and momentum fields of GATE. Part II: Parameterization. *J. Atmos. Sci.*, **46**, 1609-1629.

Tao, W.-K., and S.-T. Soong, 1986: A study of the response of deep tropical clouds to mesoscale processes: Three-dimensional numerical experiments. *J. Annos. Sci.*, **43**, 2653-2676.

Tollerud, E. I., and S. K. Esbensen, 1983: An observational study of the upper-tropospheric vorticity fields in GATE cloud clusters, *Mon. Wea. Rev.*, **111**, 2161-2175.

Thorpe, A.J., M.J. Miller and M.W. Moncrieff, 1982: Two-dimensional convection in non-constant shear: a model of midlatitude squall lines. *Quart.J.Roy.Meteor.Soc.*, **108**, 739-762.

Weisman, M. L., and J., B., Klemp, 1982: The dependence of numerically simulated convective storms on vertical wind shear and buoyancy. *Mon. Wea. Rev.*, **110**, 504-520.

----------, 1984: The structure and classification of numerically simulated convective storms in directionally varying wind shears. *Mon. Wea. Rev.*, **112**,

2479-2498.

----------, and R. Rotunno, 1988: Structure and evolution of numerically simulated squall lines. *J Atmos. Sci.*, **45**,1990-2013.

Wu X., and M., Yanai, 1994: Effects of vertical wind shear on the cumulus transport of momentum: observations and parameterization. *J. Atmos. Sci*., **51**, 1640-1660.

Yau, M. K., 1979: Perturbation pressure and cumulus convection. *J. Atmos. Sci*., **36**, 690-694.

Zhang, G. J., and H.-R. Cho, 1991a: Parameterization of the vertical transport of momentum by cumulus clouds. Part I: Theory. *J. Atmos. Sci.*, **48**, 1483-1492.

----------, and----------, 1991b: Parameterization of the vertical transport of momentum by cumulus clouds. Part II: Application. *J. Atmos. Sci*., 48, 2448-2457.

----------, and N. A. McFarlane, 1995: Role of convective scale momentum transport in climate simulation. *J. Geophys. Res.*, 100, 1417-1426.

Table 1: Criterion to distinguish various types of MCSs

	$\left\|N_1^2\right\|$ s^{-2}	vertical wind shear
Linear MCSs Type II	$\left\|N_1^2\right\| > -5\times10^{-5}$	$\left\|\frac{L_T}{L_P}\right\| < 0.1$ or $\left\|\frac{L_P}{L_T}\right\| > 10$
Linear MCSs Type I	$\left\|N_1^2\right\| < -5\times10^{-5}$	$\left\|\frac{L_T}{L_P}\right\| < 0.1$ or $\left\|\frac{L_P}{L_T}\right\| > 10$
Linear MCSs no preferred orientation	$\left\|N_1^2\right\| \approx -5\times10^{-5}$	$\left\|\frac{L_T}{L_P}\right\| < 0.1$ or $\left\|\frac{L_P}{L_T}\right\| > 10$
Nonlinear MCSs	unstable	$\left\|\frac{L_T}{L_P}\right\| > 0.1$ or $\left\|\frac{L_P}{L_T}\right\| < 10$

Figure Captions

Figure 1: **Shape of the organized convective clouds (general case).**

Figure 2: **Observed precipitation during the simulation period (**mm hour^{-1}**).**

Figure 3: **(a) Organized cumulus cloud orientation from the theory for July 15, 12:14, 1997 (Case 1), The ellipse's long axis makes an angle of 0° with the y axis. and (b) Observed rain-band.**

Figure 4: **(a) Observed rain-band for June 26, 14:30, 1997 (Case 2) and (b) Organized cumulus cloud orientation from the theory, the ellipse's long axis makes an angle of 15° with the y axis.**

Figure 5: **(a) Observed rain-band for June 26, 8:45 AM, 1997 (Case 3), and (b) Organized cumulus cloud orientation from the theory, The model regards the organized clouds as a circular mass.**

Figure 6: **(a), (b) are environmental u, v momentum (**$\mathrm{m\ s^{-1}}$**, yellow line) and their tendencies (**$\times 10^5 \mathrm{m\ s^{-2}}$**, MR runs the blue line, CR runs the red line) on June 26, 8:45 AM, 1997 (Case 3).**

Figure 7: **(a), (b) are environmental u, v momentum (**$\mathrm{m\ s^{-1}}$**, yellow line) and their tendencies (**$\times 10^5 \mathrm{m\ s^{-2}}$**, MR runs the blue line, CR runs the red line) on July 15, 12:15, 1997 (Case 1).**

Figure 8: **(a), (b) are environmental u, v momentum (**$\mathrm{m\ s^{-1}}$**, yellow line) and their tendencies (**$\times 10^5 \mathrm{m\ s^{-2}}$**, MR runs the blue line, CR runs the red line) on June 26, 14:30, 1997 (Case 2)**

Figure 1

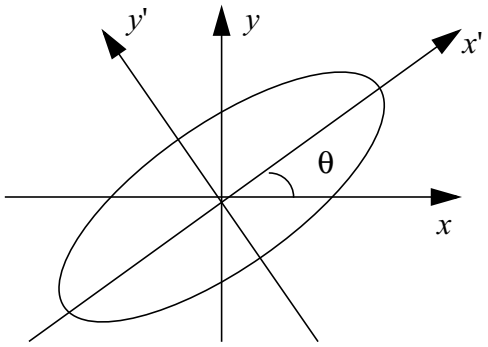


Figure 2

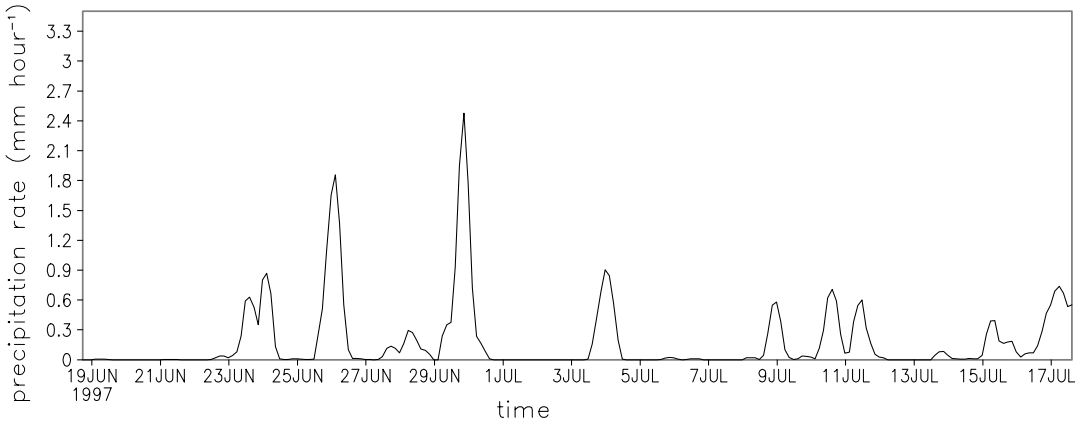
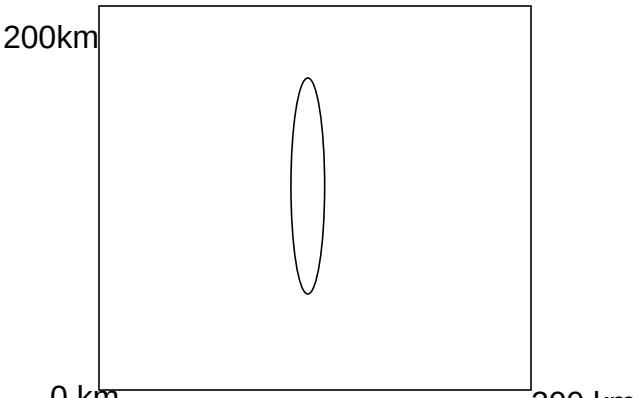
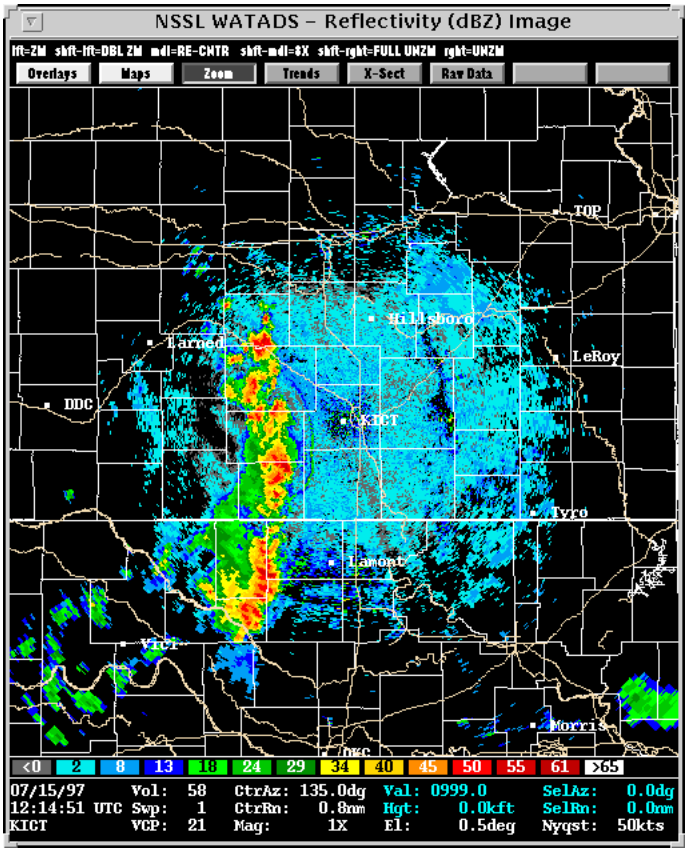


Figure 3

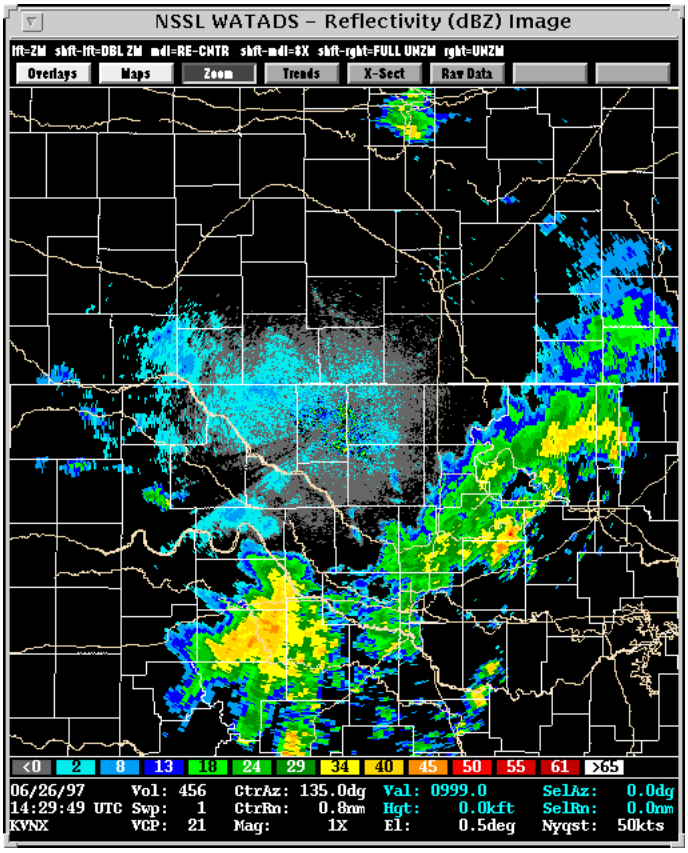

200km
0 km
200 km

(a)

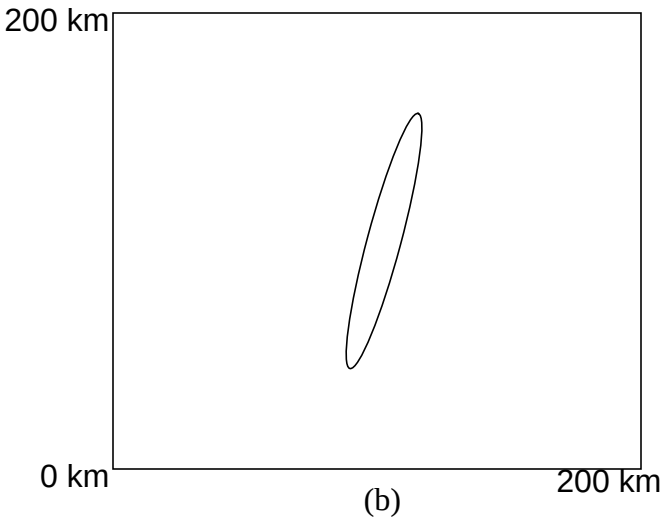

NSSL WATADS – Reflectivity (dBZ) Image
lft=ZM shft-lft=DBL ZM mdl=RE-CNTR shft-mdl=8X shft-rght=FULL UNZM rght=UNZM
Overlays
Maps
Zoom
Trends
X-Sect
Raw Data
TOP
Hillsboro
Larned
LeRoy
DDC
KICT
Tyro
Lamont
Vict
Morri
OKC
<0
2
8
13
18
24
29
34
40
45
50
55
61
>65
07/15/97 Vol: 58 CtrAz: 135.0dg Val: 0999.0 SelAz: 0.0dg
12:14:51 UTC Swp: 1 CtrRn: 0.8nm Hgt: 0.0kft SelRn: 0.0nm
KICT VCP: 21 Mag: 1X El: 0.5deg Nyqst: 50kts

(b)

Figure 4

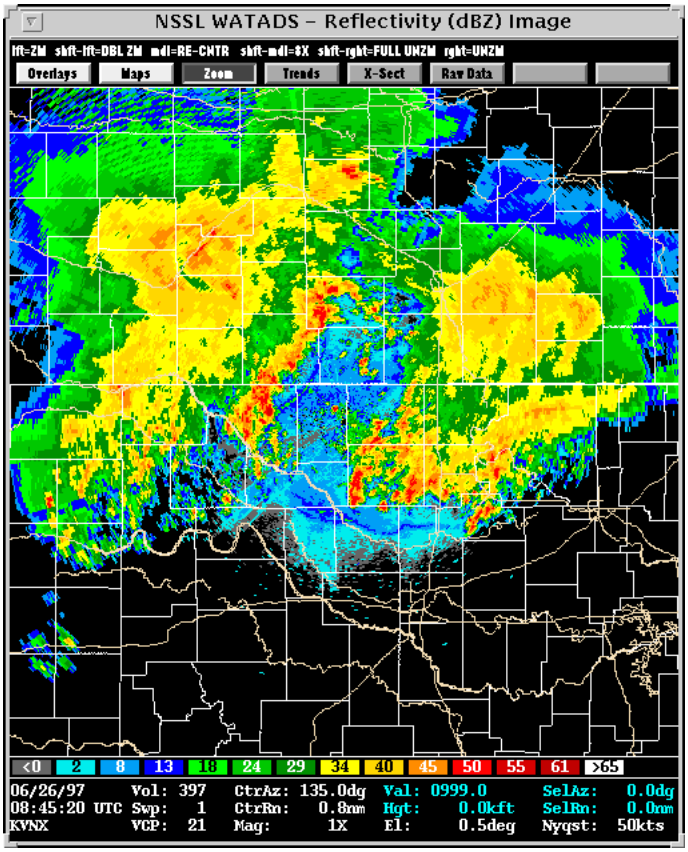

NSSL WATADS – Reflectivity (dBZ) Image
lft=ZM shft-lft=DBL ZM mdl=RE-CNTR shft-mdl=8X shft-rght=FULL UNZM rght=UNZM
Overlays
Maps
Zoom
Trends
X-Sect
Raw Data
<0 2 8 13 18 24 29 34 40 45 50 55 61 >65
06/26/97 Vol: 456 CtrAz: 135.0dg Val: 0999.0 SelAz: 0.0dg
14:29:49 UTC Swp: 1 CtrRn: 0.8nm Hgt: 0.0kft SelRn: 0.0nm
KVNX VCP: 21 Mag: 1X El: 0.5deg Nyqst: 50kts

(a)

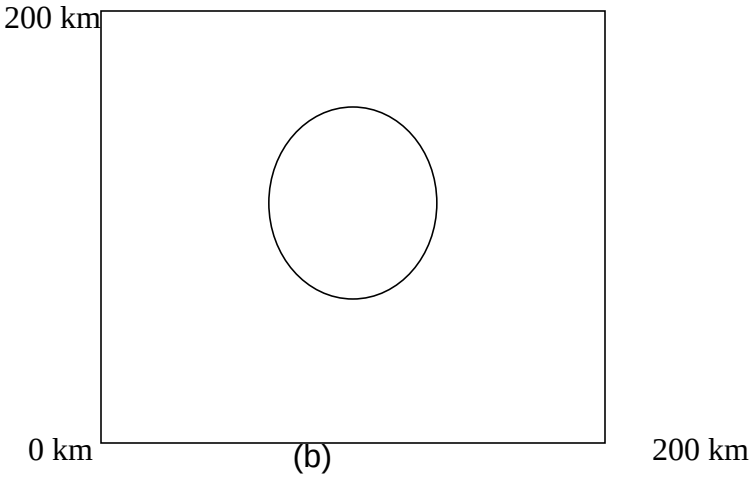

200 km
0 km
200 km

(b)

Figure 5


NSSL WATADS – Reflectivity (dBZ) Image
lft=ZM shft-lft=DBL ZM mdl=RE-CNTR shft-mdl=8X shft-rght=FULL UNZM rght=UNZM
Overlays
Maps
Zoom
Trends
X-Sect
Raw Data
<0
2
8
13
18
24
29
34
40
45
50
55
61
>65
06/26/97 Vol: 397 CtrAz: 135.0dg Val: 0999.0 SelAz: 0.0dg
08:45:20 UTC Swp: 1 CtrRn: 0.8nm Hgt: 0.0kft SelRn: 0.0nm
KVNX VCP: 21 Mag: 1X El: 0.5deg Nyqst: 50kts

(a)


200 km
0 km
200 km

(b)

Figure 6

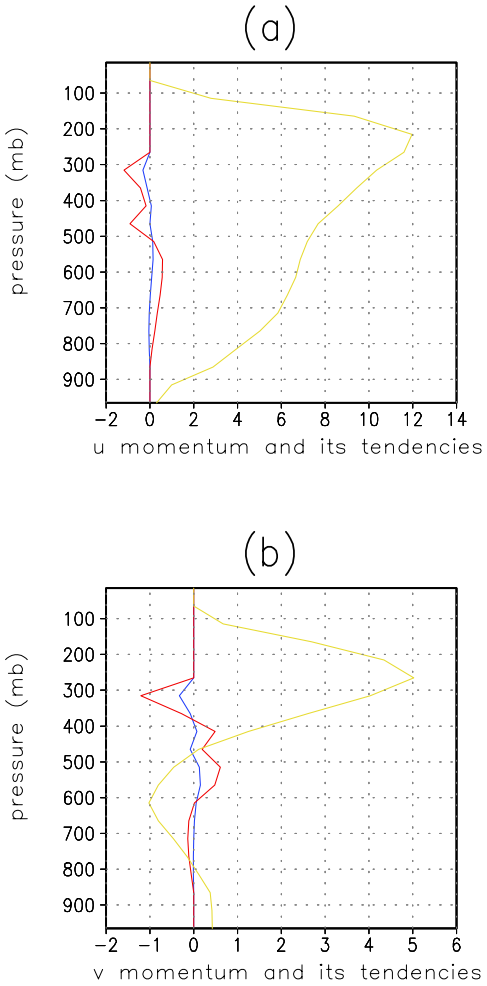

(a)
pressure (mb)
100
200
300
400
500
600
700
800
900
−2
0
2
4
6
8
10
12
14
u momentum and its tendencies
(b)
pressure (mb)
100
200
300
400
500
600
700
800
900
−2
−1
0
1
2
3
4
5
6
v momentum and its tendencies

Figure 7

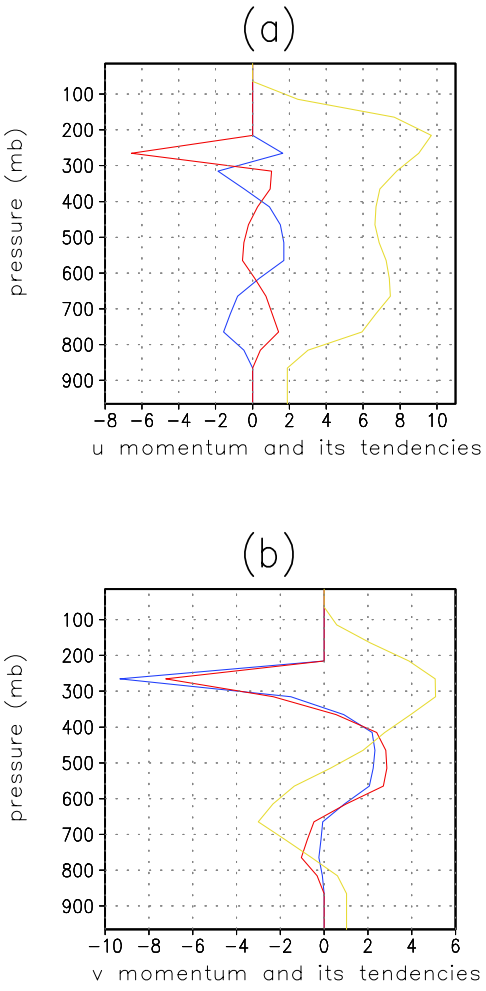
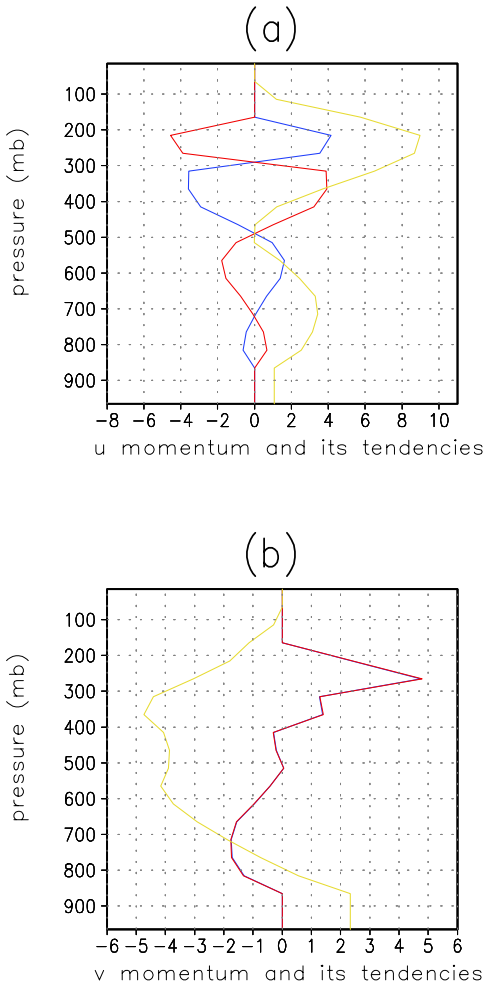

(a)
pressure (mb)
100
200
300
400
500
600
700
800
900
−8 −6 −4 −2 0 2 4 6 8 10
u momentum and its tendencies
(b)
pressure (mb)
100
200
300
400
500
600
700
800
900
−10 −8 −6 −4 −2 0 2 4 6
v momentum and its tendencies

Figure 8


(a)
pressure (mb)
100
200
300
400
500
600
700
800
900
−8 −6 −4 −2 0 2 4 6 8 10
u momentum and its tendencies
(b)
pressure (mb)
100
200
300
400
500
600
700
800
900
−6 −5 −4 −3 −2 −1 0 1 2 3 4 5 6
v momentum and its tendencies